$Cu(Mn_{0.748}Ni_{0.252})_2O_4/SiO_2$ Nanoparticle Layers for Wide-Angle Spectral Selectivity and High Thermal Stability

M. Shiva Prasad[†, ‡], B. Sobha[‡], Koppoju Suresh[†] and Shanmugasundaram Sakthivel[*, †]

[†]Centre for Solar Energy Materials, International Advanced Research Centre for Powder Metallurgy and New Materials, Balapur PO, Hyderabad - 500005, Telangana, India.

[‡]Department of Physics, National Institute of Technology, Warangal-506004, Telangana, India.

***Corresponding Author**

Tel.: +91-40-24452454, Fax: +91-40-24442699

Mail: ssakthivel@arci.res.in

Supporting Information:

S1: Elemental mappings of the spinel nanoparticle cluster

In order to understand the spatial distribution of elements across the spinel absorber film, an elemental mapping has been done on a cluster of spinel nanoparticles. Fig. S1 illustrates the elemental mappings of the spinel nanoparticle cluster by TEM.

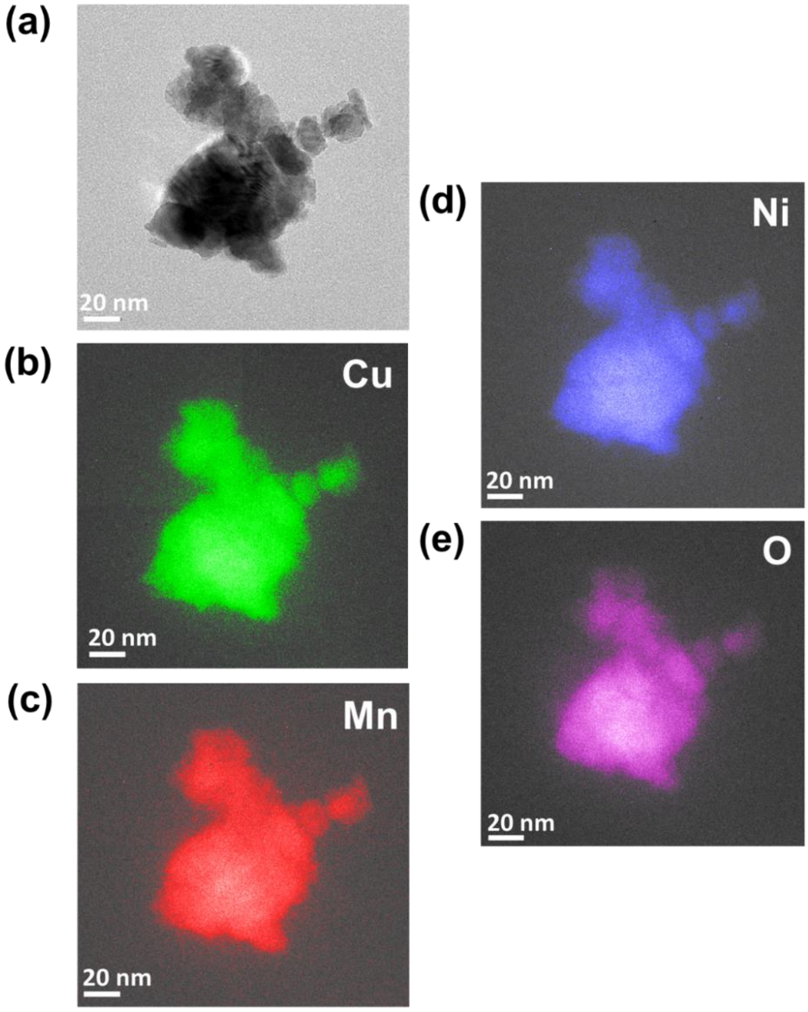

Figure S1. Chemical analysis of spinel structured nanoparticles cluster (a) TEM micrograph spinel nanoparticles (b) Copper (c) Manganese (d) Nickel (e) Oxygen elemental mappings

S2. Measurement of Refractive index for dual-functional layer:

The variable angle spectroscopic ellipsometry is utilized to measure the refractive index(η) and the thickness of the dual-functional layer. At first, the phase change measured for the dual-functional layer coated glass substrates (with 1 mm/sec) in the region of 400-1700nm and collected ψ and Δ to build a model. The Cauchy model used for the fitting of optical constants with the aid of experimentally obtained ψ and Δ values (Fig.S2). Finally, the refractive index of the dual-functional layer found out to be 1.32 at 550nm. Data fitting was done to find out the best fit between the generated and measured data. The Mean Squared Error (MSE) is used to quantify the difference between a generated and the measured data. A low MSE implies a good match between the model and experiment. The mean squared error (MSE) value of the fitted result is only 1.353 (Fig.S3), which illustrates that the simulated optical constants is reliable due to the small value.

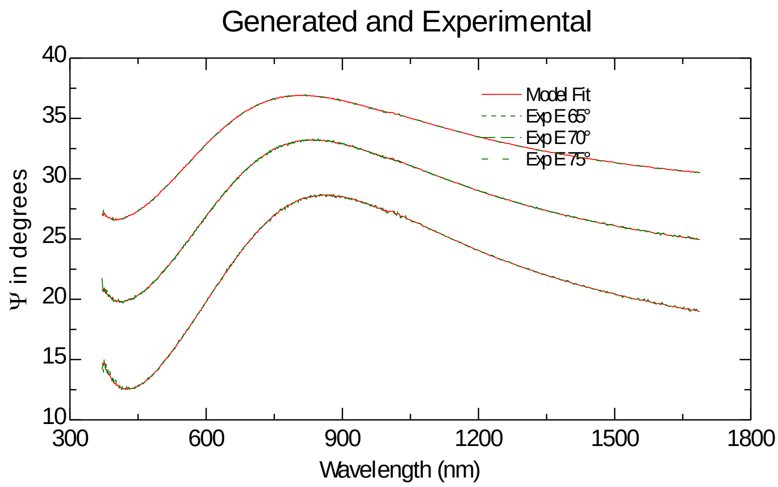

Figure S2. Generated and experimental data fitting using Cauchy model for dual-functional layer over on soda lime glass.

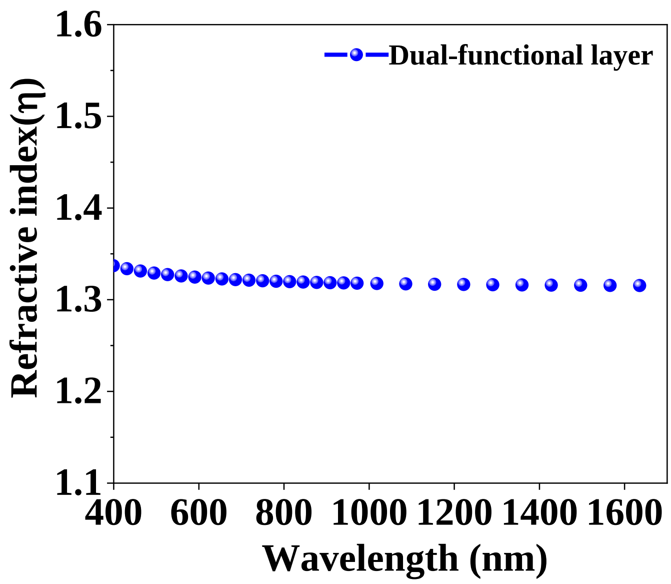

Figure S3. Refractive index of dual-functional layer

S3. GIXRD study: The bare SS 304, annealed SS 304 at 500 °C, spinel and tandem absorbers were analyzed by GIXRD to determine the phase structure. Fig. S4 represents the GIXRD pattern of bare SS 304, annealed SS 304, spinel and tandem absorbers, respectively.

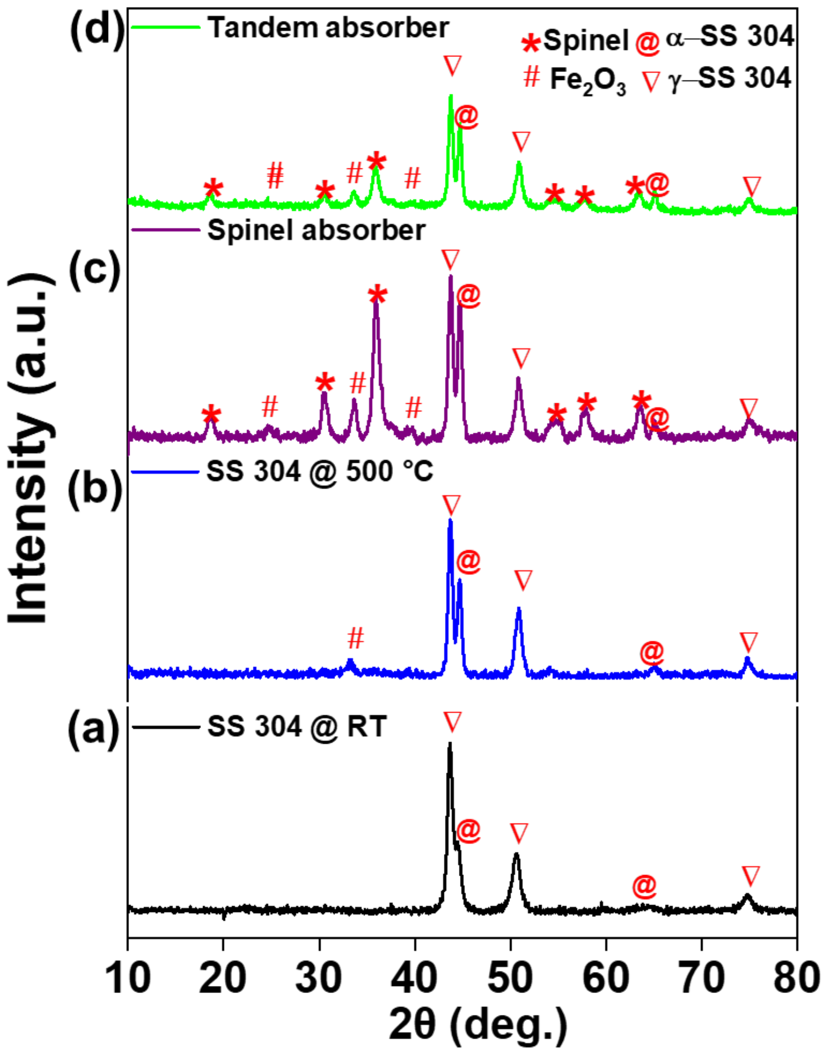

Figure S4. GIXRD pattern of (a)SS 304, (b)annealed SS 304 at 500 °C, (c)spinel absorber (SS/Cu$(Mn_{0.748}Ni_{0.252})_2O_4$) and (d)tandem absorber (SS/Cu$(Mn_{0.748}Ni_{0.252})_2O_4/SiO_2$) at an optimum glazing incidence angle (0.5°).

S4. Morphology and thickness study of spinel absorber:

The developed spinel absorbers were studied by FESEM to understand the morphology and to determine the thickness of the optimized coating. Fig. S5(a) and (b) represent the morphology and thickness of the spinel absorber layer.

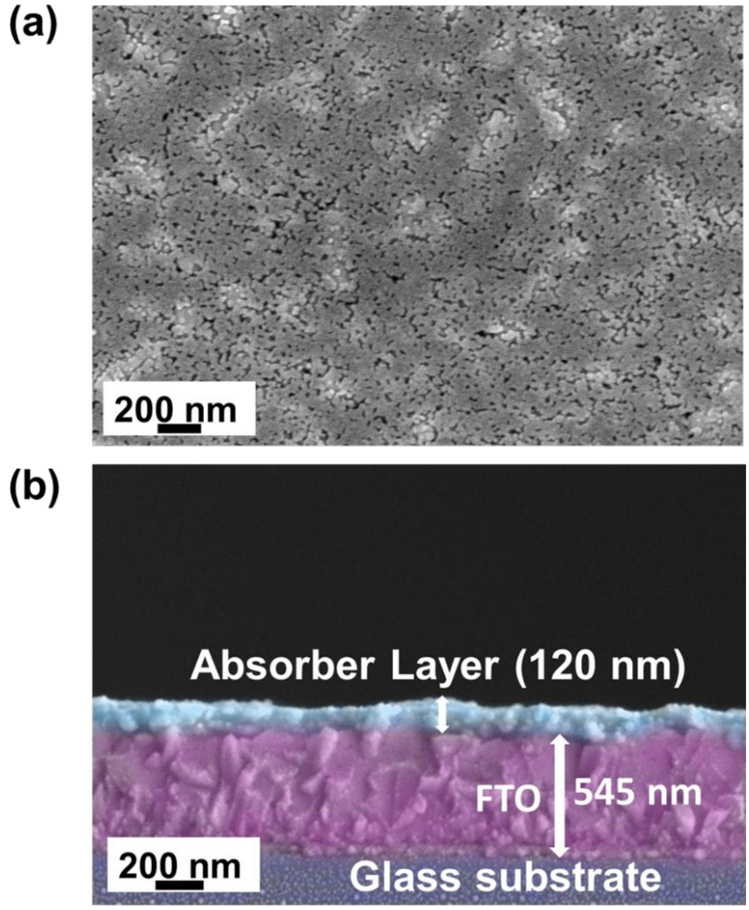

Figure S5. (a) Morphology and (b) FESEM cross-section image of spinel absorber layer coated over on an FTO glass substrate

S5. Morphology and thickness study of dual-functional layer:

The dual-functional layer is studied by FESEM to understand the morphology and to determine the thickness of the optimized coating. Fig. S6(a) and (b) represent the morphology and thickness of the dual-functional layer.

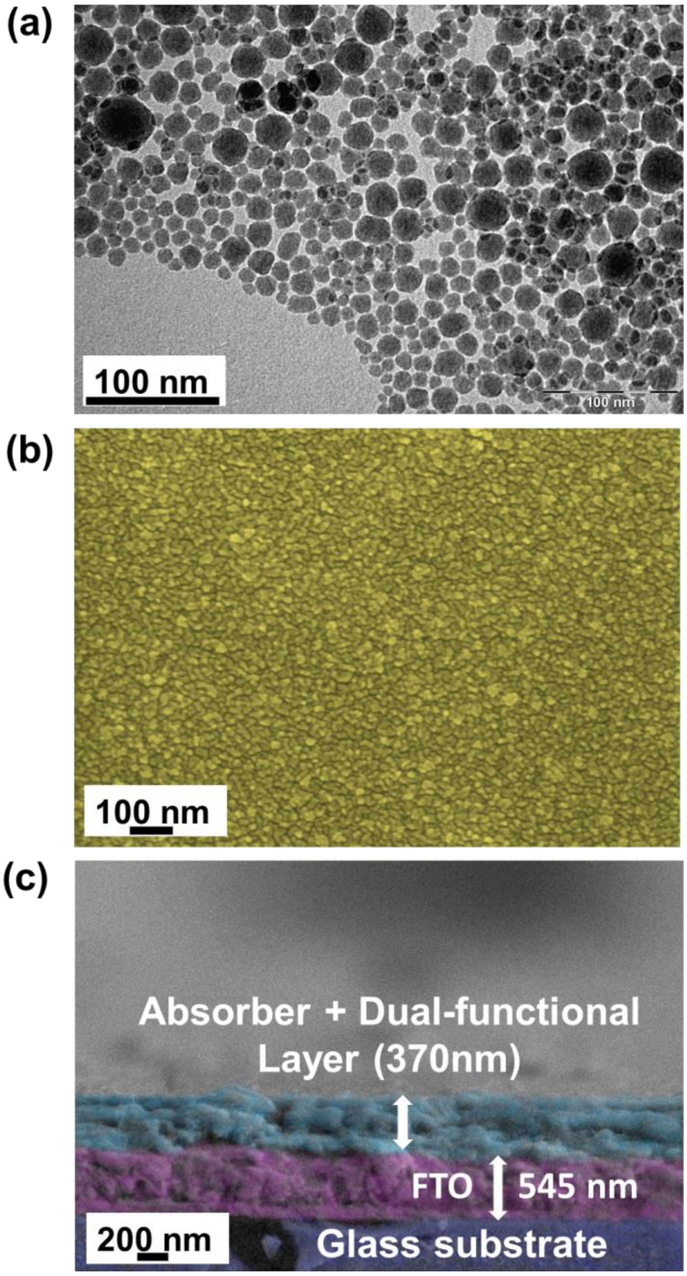

Figure S6. (a)TEM micrograph of SiO_2 nanoparticles (b) morphology (c) FESEM cross-section image of dual functional layer coated over on a spinel absorber

S6. Thermal loss study of spinel and tandem absorber:

The spinel and tandem absorbers were measured by the FTIR spectrophotometer to estimate the thermal emissivity from 100 °C to 500 °C. The thermal emissivity spectra of both spinel and tandem absorber samples were presented in Fig. S7(a) & (b) and values at temperatures from 100 °C to 500 °C were mentioned in table S1.

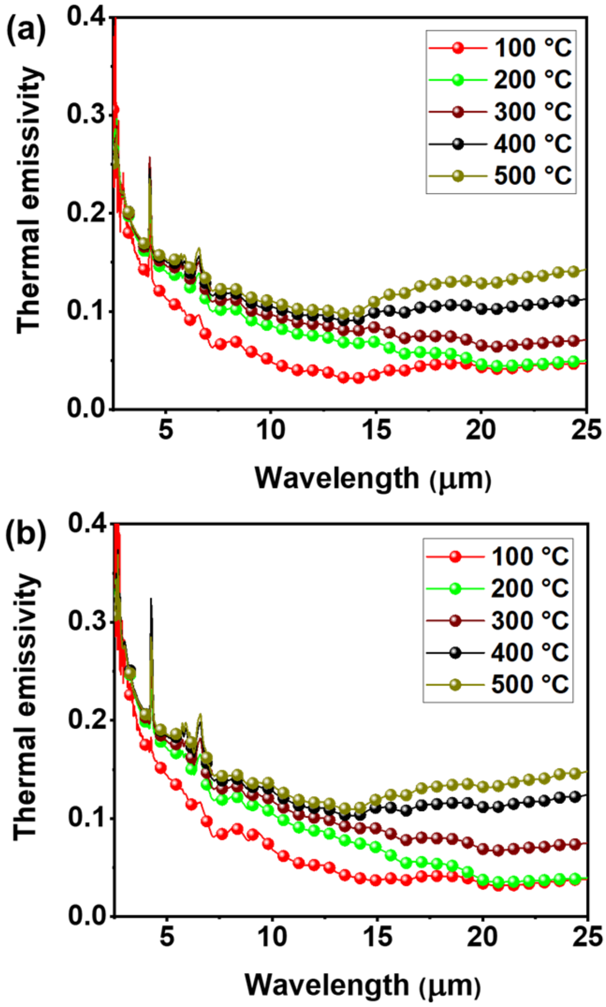

Figure S7. The thermal emissivity spectra of (a) spinel absorber (b) tandem absorber

Table S1. The thermal emissivity of spinel absorber and tandem absorber at optimized withdrawal speeds

Temperature (°C)	Spinel absorber	Tandem absorber
100	0.06	0.07
200	0.07	0.09
300	0.10	0.11
400	0.12	0.13
500	0.13	0.15

S7. Adhesion of spinel and tandem absorber:

In order to understand the adhesion of developed coatings, we used Cross-cut test according to ASTM standard D3359–09. As per standard, we made an X-cut of length (40mm) with a sharp knife through the absorber and tandem films to the substrate at an angle of 30-45 °. Further, 75mm long pressure sensitive tape applied over on an incision area and rubbed firmly with the eraser on the end of a pencil. After 90 seconds, removed the tape rapidly by holding the free end.

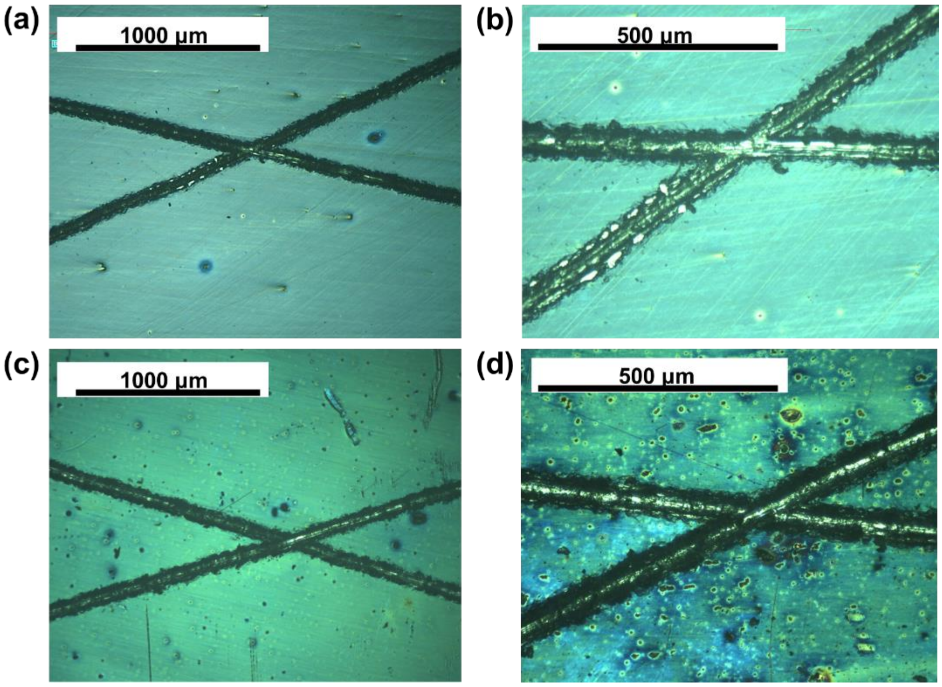

Figure S8. Optical microscope images of (a) & (b) spinel absorber and (c) & (d) tandem absorber at different magnifications.

Furthermore, we examined the samples carefully before and after tape test under optical microscope to estimate the adhesion rate. From Fig. S8, we can observe that there is trace peeling of both coatings along the incisions. Hence, the rate of adhesion for spinel and tandem absorber is 4.

Table S2. Solar absorptance of spinel absorber and tandem absorber at different incident angles

Incident angle (°)	10	20	30	40	50	60	70	80
Spinel absorber	91.0	90.3	88.6	85.5	80.6	72.5	59.0	37.0
Tandem absorber	95.6	95.4	95.1	94.5	93.4	90.9	84.2	64.6

Table S3:

Solar absorptance (α) and thermal emittance (ε) of the spinel absorber and tandem absorbers cured in air at 500 °C for 250 h with 50h interval.

Sample	Spinel absorber		Tandem absorber	
	α	ε	α	ε
as-prepared	0.882	0.145	0.95	0.14
ann_50h	0.856	0.154	0.952	0.141
ann_100h	0.852	0.163	0.955	0.143
ann_150h	0.845	0.171	0.955	0.146
ann_200h	0.844	0.185	0.957	0.148
ann_250h	0.845	0.192	0.956	0.149

Table S4:

Solar absorptance of spinel absorber and tandem absorber at different incident angles after thermal stability study

Incident angle (°)	**10**	**20**	**30**	**40**	**50**	**60**	**70**	**80**
Spinel absorber	92.4	91.6	90	87.3	82.9	75.4	62.6	42
Tandem absorber	96.8	96.5	96.1	95.1	93.2	89	79.8	58.3